Supporting information

Mesoporous Paladium-Copper Bimetallic Electrodes for Selective Electrocatalytic Reduction of Aqueous CO_2 to CO

Mu Li,[a,b⊥] Junjie Wang,[a⊥] Peng Li,[a] Kun Chang,[a] Cuiling Li,[a] Tao Wang,[a] Bo Jiang,[a] Huabin Zhang,[a] Huimin Liu,[a] Yusuke Yamauchi,[a,c] Naoto Umezawa*[a,b,c] and Jinhua Ye*[a,b,c,d]

[a]Environmental Remediation Materials Unit and International Center for Materials Nanoarchitectonics (MANA), National Institute for Materials Science

1-1 Namiki, Tsukuba, Ibaraki 305-0044 (Japan) E-mail: Jinhua.YE@nims.go.jp; UMEZAWA.Naoto@nims.go.jp

[b]Graduate School of Chemical Science and Engineering, Hokkaido University,

Sapporo 060-0814 (Japan)

[c]TU-NIMS Joint Research Center, School of Material Science and, Engineering, Tianjin University, 92 Weijin Road, Tianjin (P.R. China)

[d]Collaborative Innovation Center of Chemical Science and Engineering (Tianjin), Tianjin 300072, P. R. China.

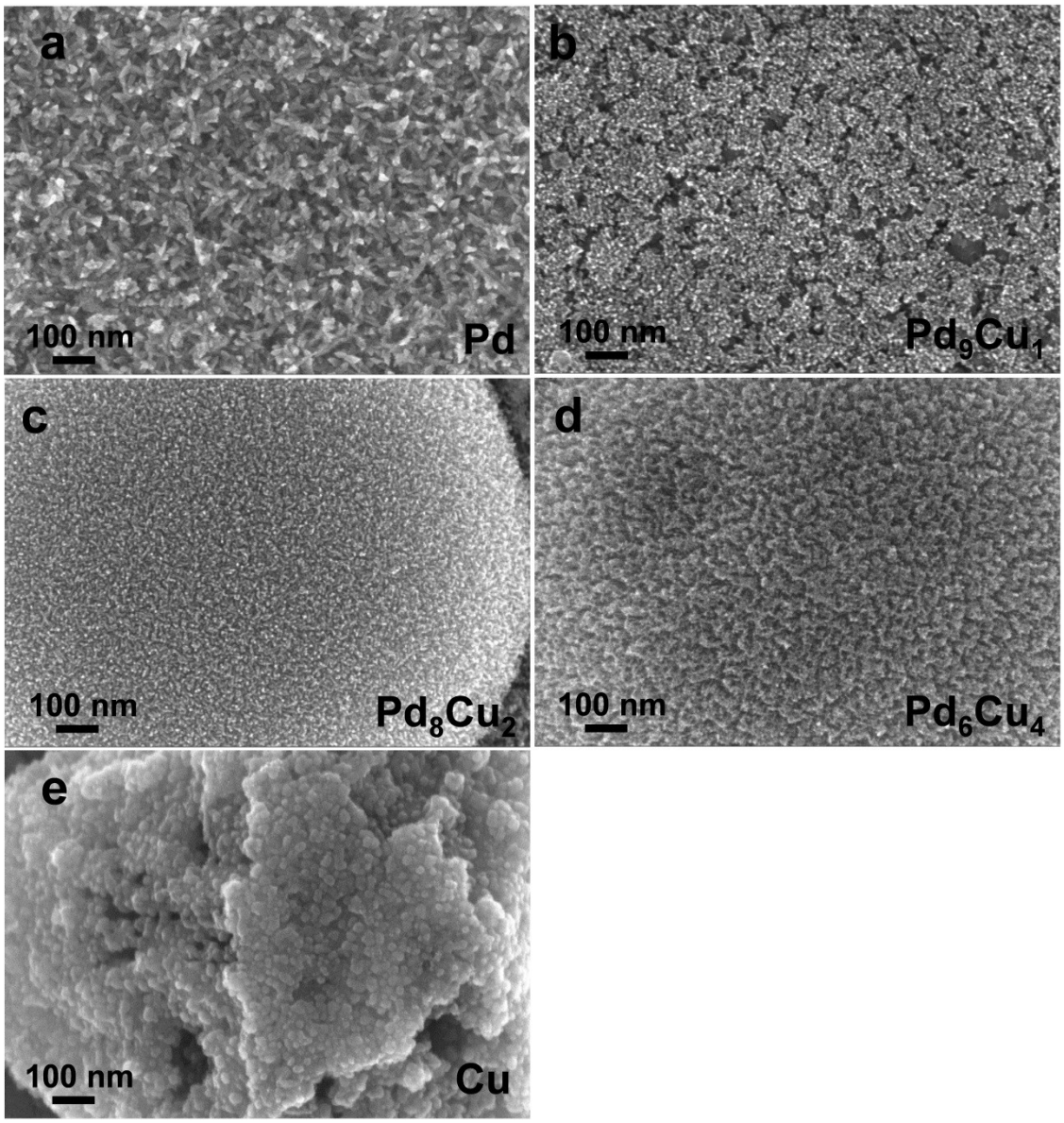

Figure S1: Top-surface SEM images of mesoporous Pd-Cu electrocatalysts with different ratios: a) Pd, b) Pd_9Cu_1, c) Pd_8Cu_2, d) Pd_6Cu_4 and e) Cu.

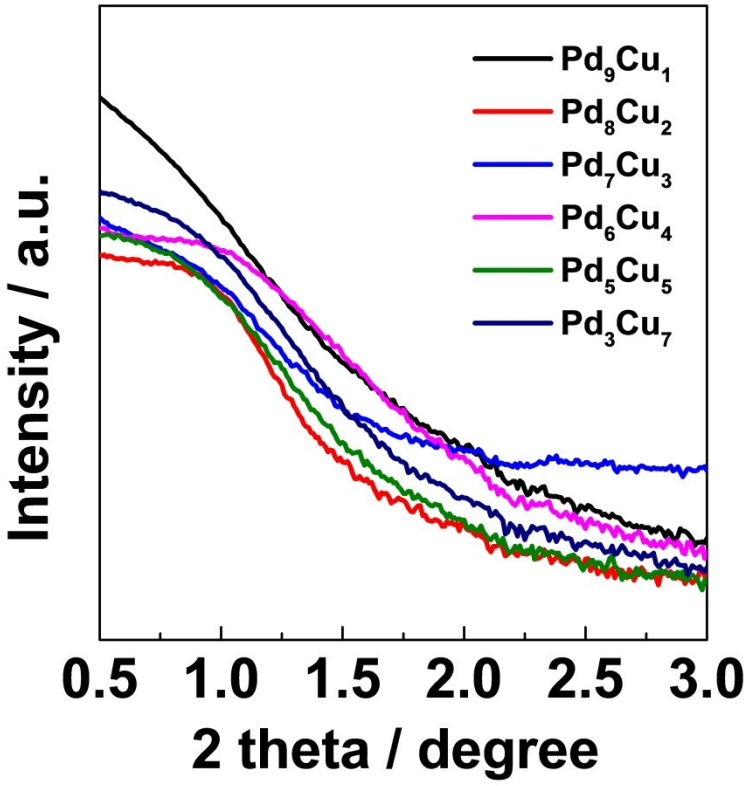

Figure S2: Low-angle XRD patterns of mesoporous Pd-Cu electrocatalysts with different ratios.

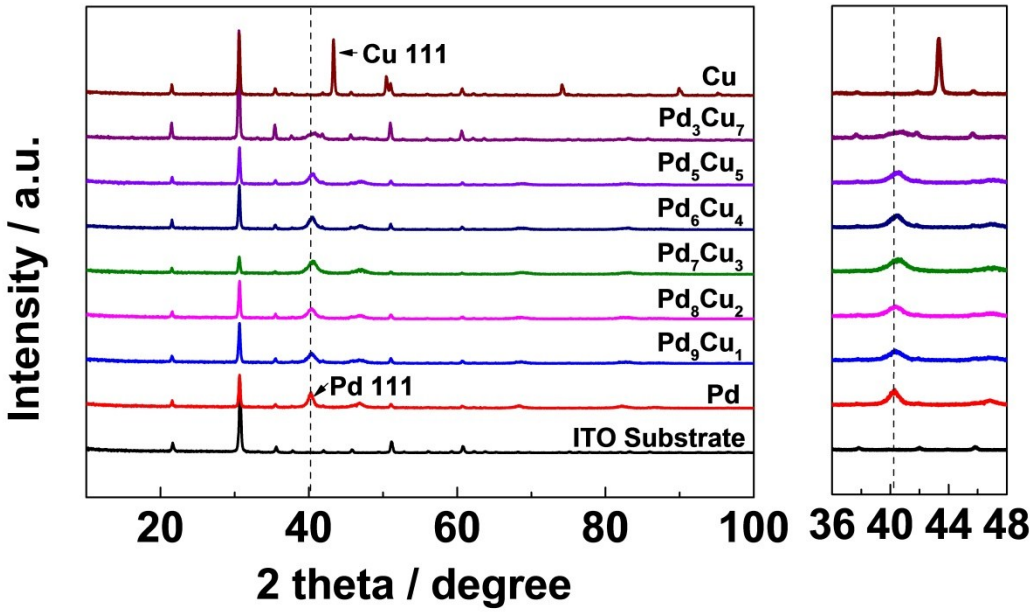

Figure S3: XRD patterns of mesoporous Pd-Cu electrocatalysts with different ratios.

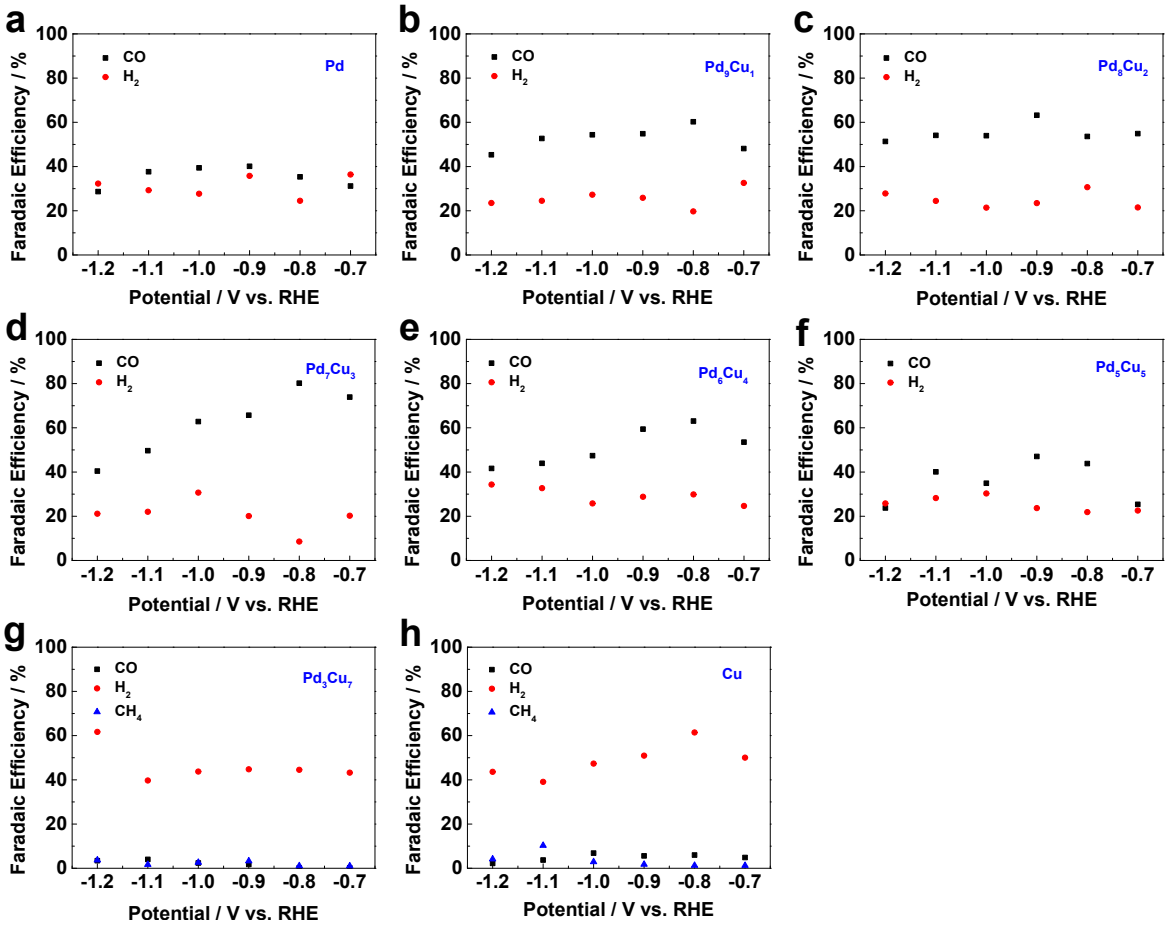

Figure S4: Faradaic efficiencies of the series of mesoporous paladium-copper bimetallic electrocatalysts for the two main products of CO and H_2: a) Pd, b) Pd_9Cu_1, c) Pd_8Cu_2, d) Pd_7Cu_3, e) Pd_6Cu_4, f) Pd_5Cu_5, g) Pd_3Cu_7 and h) Cu.

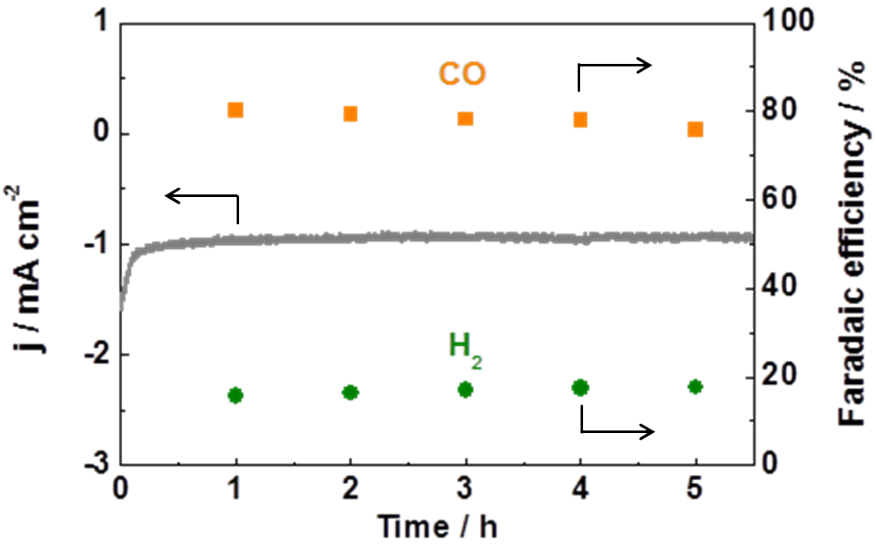

Figure S5: Durability text over mesoporous Pd_7Cu_3 alloy at -0.8 V *vs.* RHE.

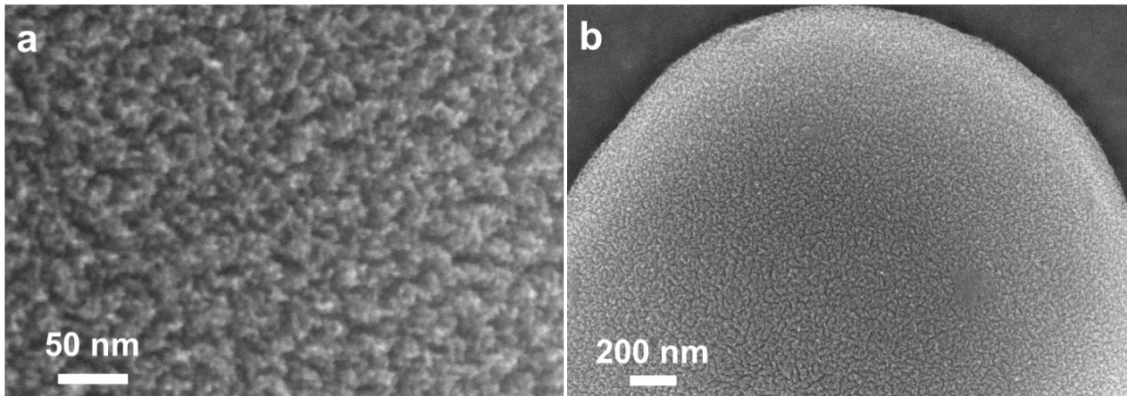

Figure S6: a) and b) Top-surface SEM images of mesoporous Pd_7Cu_3 alloy after electrochemical measurements.

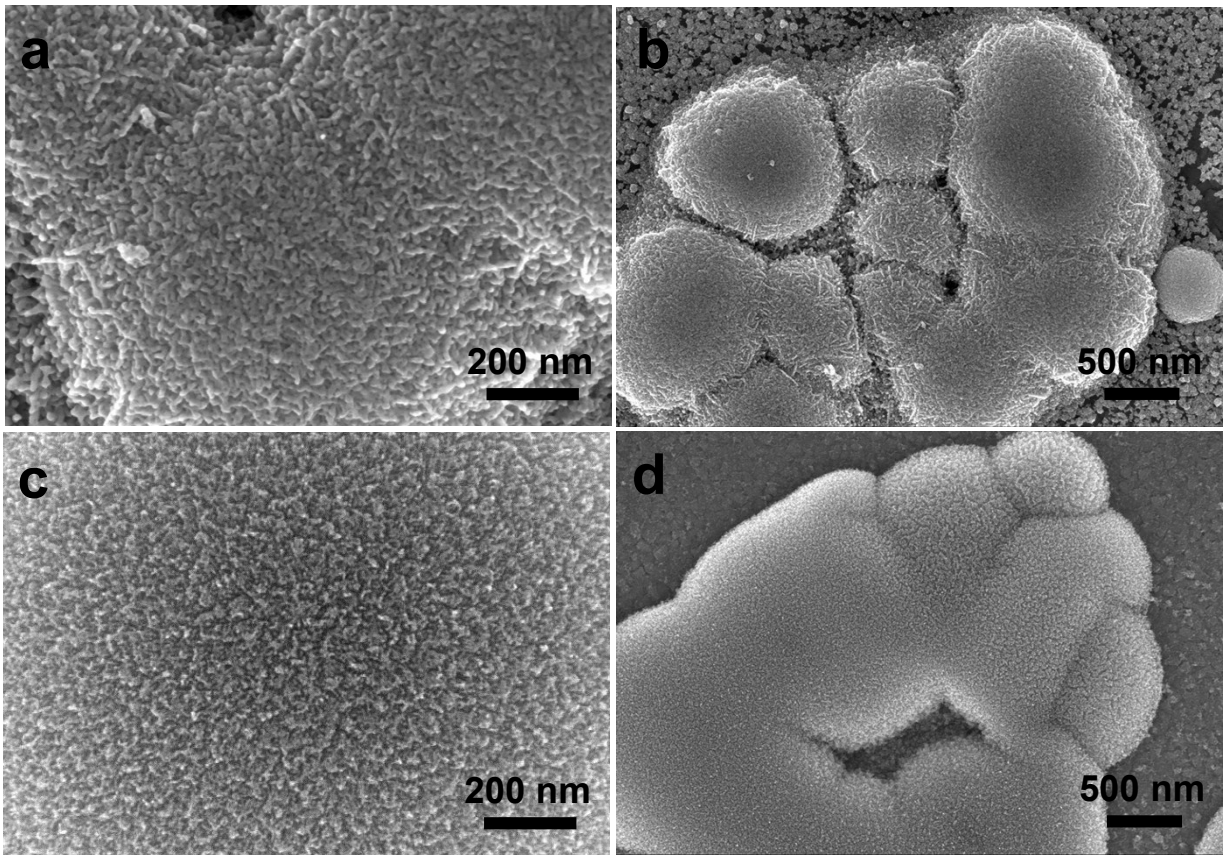

Figure S7: Top-surface SEM images of a) and b) N-Pd_7Cu_3 prepared without surfactant; c) and d) M-Pd_7Cu_3 prepared with surfactant.

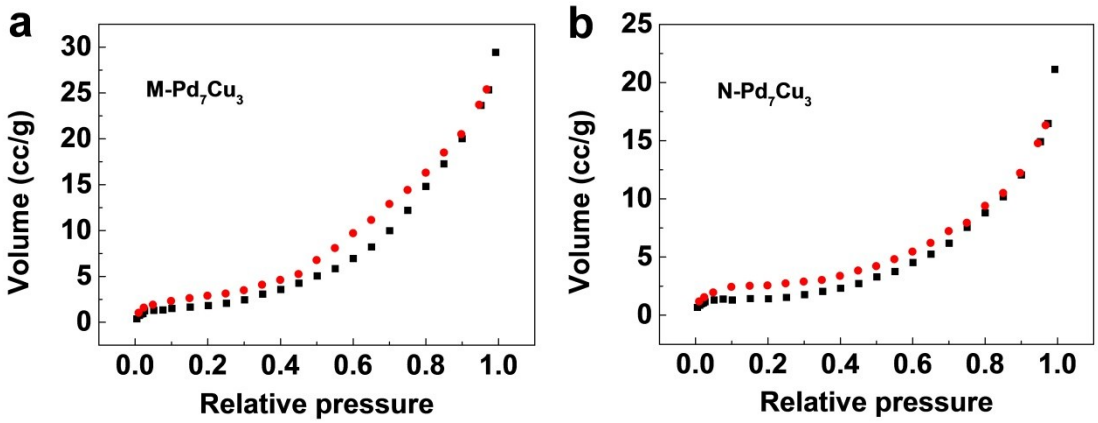

Figure S8: Nitrogen adsorption-desorption isotherm of a) mesoporous Pd_7Cu_3 (17.6 m^2 g^{-1}) and b) nanoparticle Pd_7Cu_3 (9.6 m^2 g^{-1}).

Contents in Figure S8

The detected specific surface area of mesoporous Pd_7Cu_3 (17.6 m^2/g) exhibited similar value to the previous reported mesoporous Pt (14 ~ 22 m^2/g)[1-3].

1. S. A. G. Evans, J. M. Elliott, L. M. Andrews, P. N. Bartlett, P. J. Doyle and G. Denuault, Anal. Chem., 2002, 74, 1322-1326.

2. X. Teng, X. Liang, S. Maksimuk and H. Yang, Small, 2006, 2, 249-253.

3. S. Tominaka, C.-W. Wu, T. Momma, K. Kuroda and T. Osaka, Chem. Commun., 2008, DOI: 10.1039/B803225D, 2888-2890.

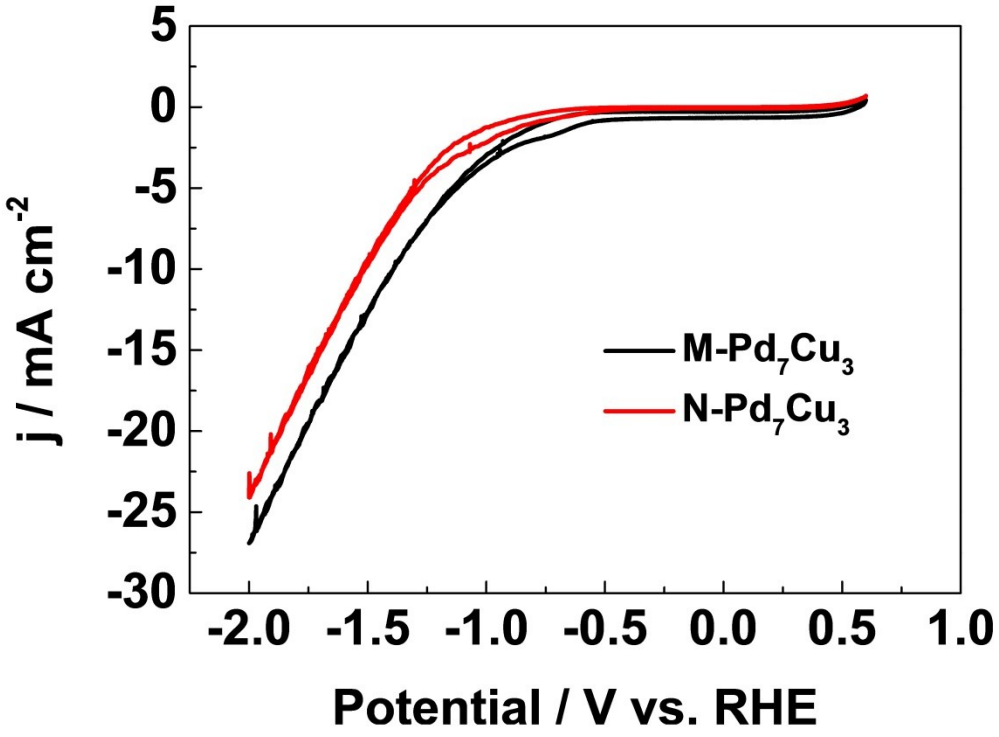

Figure S9: Cyclic voltammograms of M-Pd_7Cu_3 and N-Pd_7Cu_3 in 0.1 M CO_2 saturated $KHCO_3$ solution at a scan rate of 100 mV s^{-1} from 0.6 V to -2.0 V.

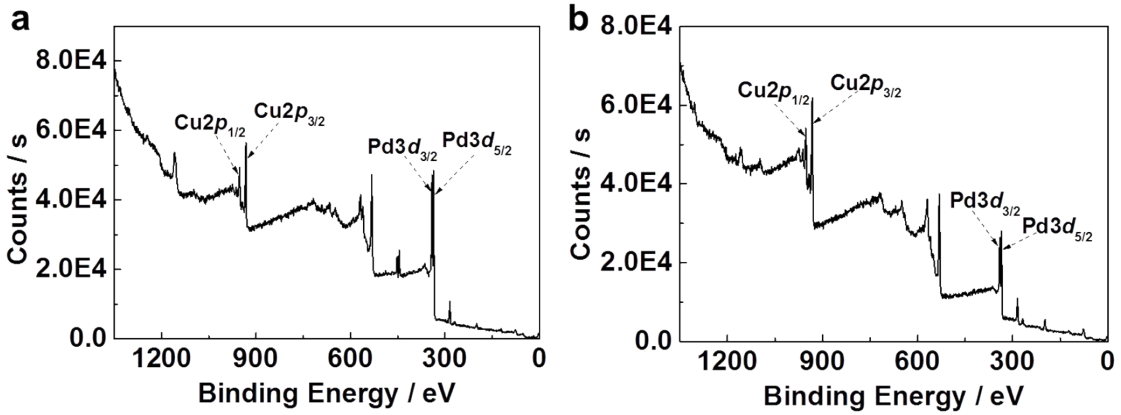

Figure S10: XPS spectra of PdCu bimetallic electrocatalysts a) with and b) without surfactant.

Contents in Figure S10

The surface composition Pd:Cu was determined as 54:46 and 30:70 for M-Pd_7Cu_3 and N-Pd_7Cu_3, respectively. Both the Pd:Cu ratios are lower than the stoichiometric concentration Pd_7Cu_3 in the starting electrolytes. The surface composition of M-Pd_7Cu_3 is also lower than the ICP-OES result (Figure 1d). It can be deduced that the total compositional ratio within the mesoporous Pd-Cu alloy accords well with the stoichiometric concentration in the starting electrolytes, while the surface composition is different from the total alloy compositional ratio. This difference can be ascribed to the deposition potential gap (E_{Pd} = 0.951V, E_{Cu} = 0.342 V) between Pd and Cu as well as the long deposition time (600 s) of our preparation process. Pd was more primarily reduced than Cu during the initial period of deposition process. With Pd concentration decreasing gradually in the electrolyte solution, more Cu became to be deposited and thus exhibited lower Pd:Cu ratio than the stoichiometric concentration 7:3 at the surface. The SEM images (Figure S1, Figure 1) shows that the mesoporous morphology highly depend on the Pd:Cu ratio. It exhibits perfect mesoporous surface when Pd is the dominant component, which can be deduced that the surfactant Brij 58 preferably interacts with Pd. So that Brij 58 could balance the deposition rate gap between Pd and Cu. Thus, the surface composition of M-PdCu (54:46) shows high Pd:Cu ratio than N-PdCu (30:70). This result also accord with the DFT calculations. Pd serves as the active centers within the PdCu alloy and the higher Pd content in M-Pd_7Cu_3 consequently lead to much better performance for reducing CO_2 to CO.

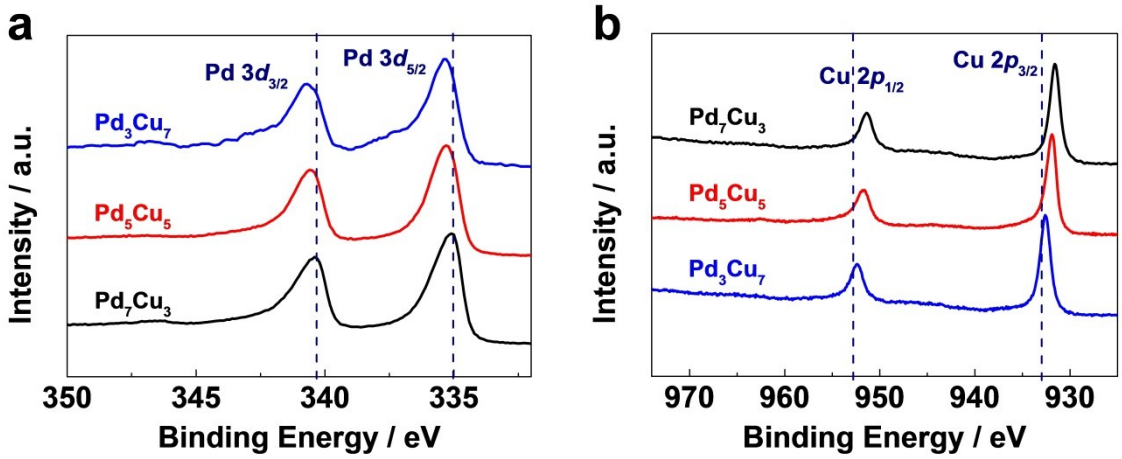

Figure S11: XPS spectra of mesoporous PdCu bimetallic electrocatalysts: a) Pd 3*d* b) Cu 2*p*. The dash line (…) marks the peak position of monometallic Pd and Cu.

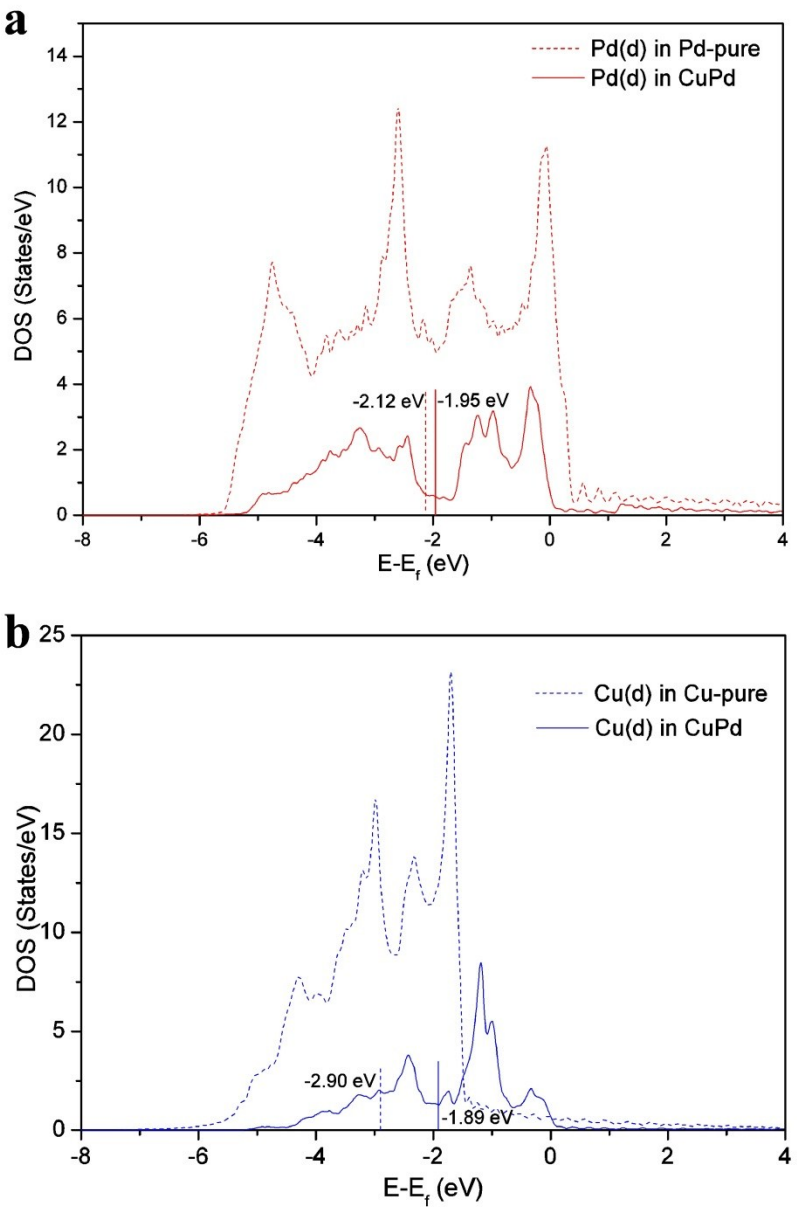

Figure S12: Projected *d*-states in CuPd, pure Pd and pure Cu: a) projected *d*-states of Pd in pure Pd and CuPd; b) projected *d*-states in pure Cu and CuPd. The positions of *d*-band centers are illustrated.

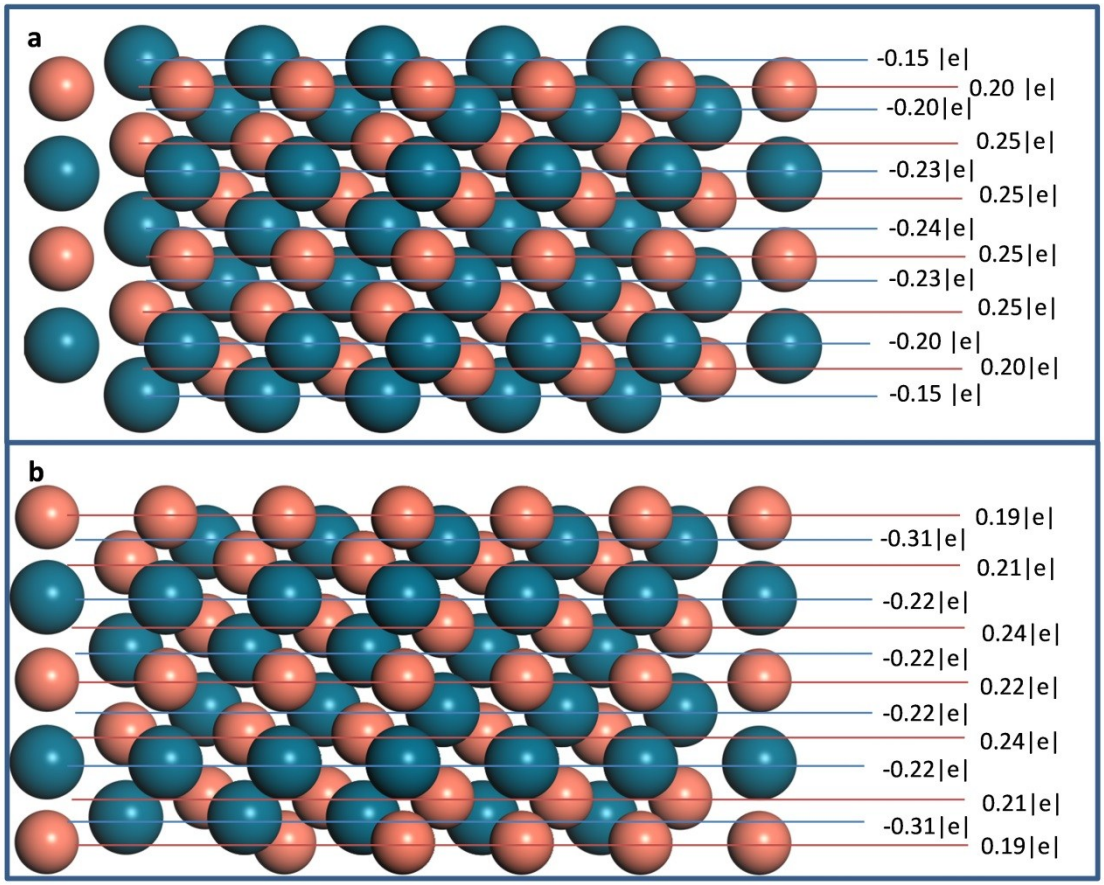

Figure S13: Calculated Bader charge difference referenced to elemental phase of each metal for the Pd- (a) and Cu-terminated (b) CuPd (111) surfaces. |e|: elementary charge

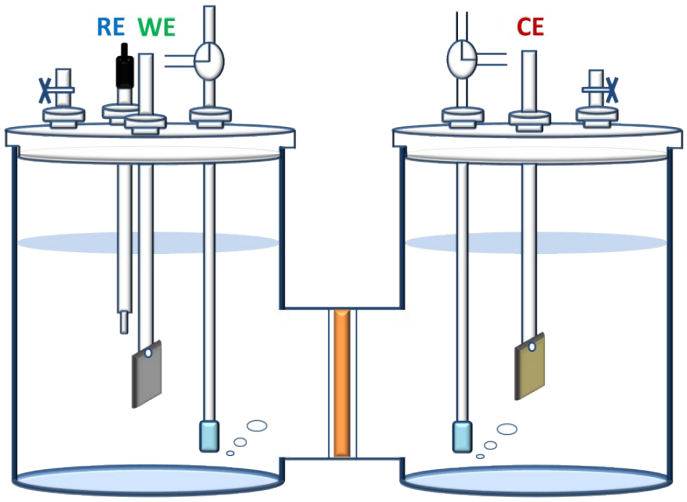

Figure S14: Schematic model of the gas-tight two compartment H-cell separated by Nafion117 film.

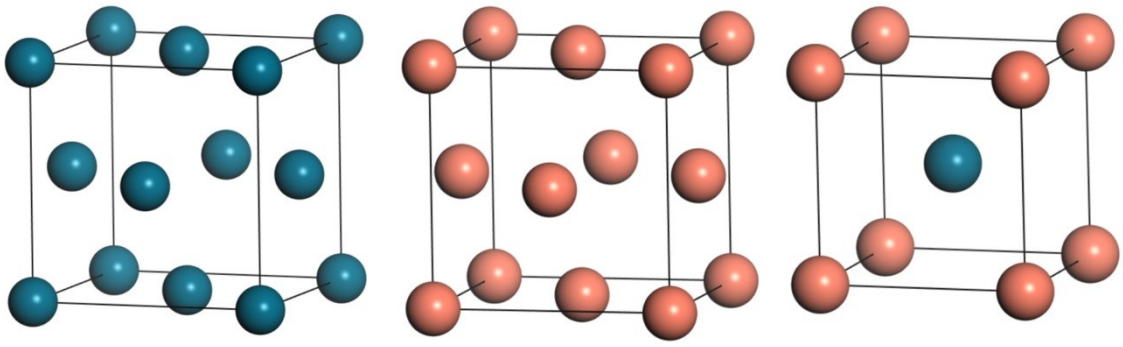

Figure S15: The crystal structures of different metals: (a) Pd, (b) Cu and (c) CuPd.

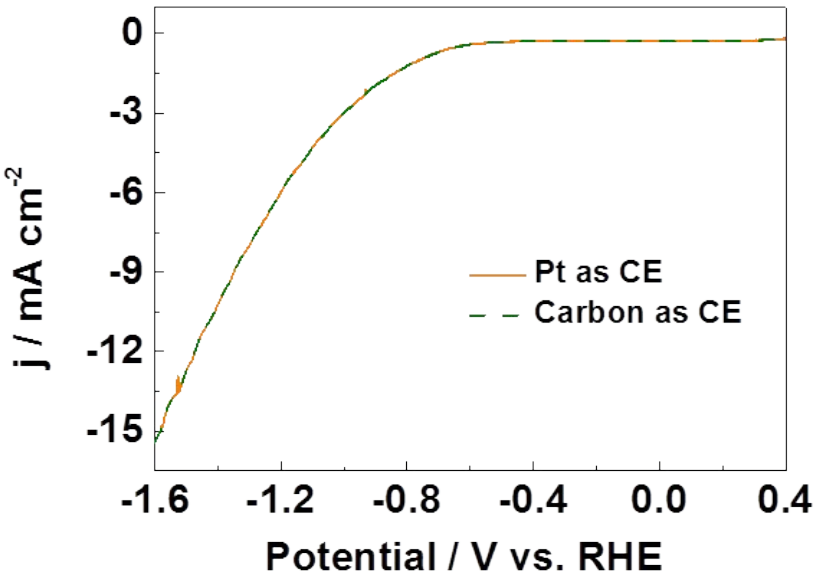

Figure S16: Comparison of Pt as counter electrode (CE) with Carbon as counter electrode.

Contents in Figure S16

The current density of Carbon CE exhibits almost identical response with the Pt CE. This can be ascribed to our measurement condition for the CO_2 reduction reaction. As shown in Figure S15, a gas-tight two compartment H-cell which is separated by a Nafion117 film was employed for all the electrochemical measurements. The WE and CE was separated by Nafion film, which suggest that only protons can transfer and exchange between the two compartments. The CE only contributed to the current by performing the oxidation half reaction and provides protons to the reduction side. In our three-electrode cell system, it mainly exhibited the catalytic performances of Pd-Cu alloy WE and so that both the Pt and Carbon CE demonstrated alike current response.

Table S1. Calculated adsorption energies for CO_2, COOH* intermediate and CO on Pd (111) facet, Pd-terminated Pd-Cu (111) facet, Cu (111) facet and Cu-terminated Pd-Cu (111) facet.

	CO_2 / eV	**COOH* / eV**	**CO / eV**
Pd (111)	**-0.065**	**-2.838**	**-2.560**
Pd-terminated Pd-Cu (111)	**-0.421**	**-3.075**	**-1.960**
Cu (111)	**-0.037**	**-2.280**	**-1.270**
Cu-terminated Pd-Cu (111)	**-2.202**	**-2.470**	**-1.840**

Table S2. Experimental and calculated lattice constants of Pd, Cu and Pd-Cu.

Metal	Space group	*a*=*b*=*c* (Å)	
		Experimental	Calculated (PBEsol)
Pd	Fm-3m	3.891	3.872
Cu	Fm-3m	3.615	3.570
Pd-Cu	Pm-3m	3.987	3.963